Title
Photocatalytic Performance of Amine-Functionalized Ti-MOF/GO Hybrids Synthesized by Microwave Route

Author
Li, Xinru

Publication Date
2016

Peer reviewed|Thesis/dissertation

UNIVERSITY OF CALIFORNIA

Los Angeles

Photocatalytic Performance of Amine-Functionalized Ti-MOF/GO Hybrids Synthesized by Microwave Route

A thesis submitted in partial satisfaction of

the requirements for the degree Master of Science

in Chemical Engineering

By

Xinru Li

2016

ABSTRACT OF THE THESIS

Photocatalytic Performance of Amine-Functionalized Ti-MOF/GO Hybrids Synthesized by Microwave Route

by

Xinru Li

Master of Science in Chemical Engineering

University of California, Los Angeles, 2016

Professor Yunfeng Lu, Chair

Graphene oxide (GO) enhanced amine-functionalized titanium metal organic framework (NH_2-MIL-125(Ti)) was fabricated via a facile microwave solvothermal process by using GO, $C_{12}H_{28}O_4Ti$, and 2-aminoterephthalic acid as precursors. Under the microwave, the surface functional group of GO could act as antenna for fast absorbing microwave energy which results hot spots on the GO sheet (hot-spots effect). These hot-spots allowed heterogeneously formation of highly-crystallized NH_2-MIL-125(Ti) nanocrystals on GO. Meanwhile, efficient electron hole separation path way was achieved, supported by XRD, Raman, UV-vis and so on. Such GO/ NH_2-MIL-125(Ti) hybrid exhibited great enhancement of visible-light absorption, photocurrent

intensity, electron carrier density and a lower photo-generated electron-hole recombination rate, compared to the pure NH_2-MIL-125(Ti). Therefore, the as-obtained hybrid system was proved highly efficient for photocatalytic oxidation of gaseous pollutants, such as nitric oxide (NO_x) and acetaldehyde with long durability, under visible light ($\lambda > 420$ nm) irradiation.

The thesis of Xinru Li is approved.

Selim M. Senkan

Robert F. Hicks

Yunfeng Lu, Committee Chair

University of California, Los Angeles

2016

DEDICATION

First and foremost, I would like to show my deepest gratitude to my supervisor, Dr. Lu, a respectable, responsible and resourceful scholar, who has provided me with valuable guidance in every stage of the writing of this thesis. His keen and passionate academic observation enlightens me not only in this thesis but also in my future study.

I shall extend my thanks to all the group members for their kindness and help. They are Dr. Huihui Zhou, Zaiyuan Le, Xiaoyan Liu, Gurong Shen, Dr. Jing Liu, Dr. Haobin Wu, Dr. Yang Liu, Dr. Jian Zhu, Dr. Zhengyin Wu, Dr. Yurong Ren, Dr. Yunfei Ma, Li Shen, Xianyang Li, Zhuang Liu, Xiaoqiong Bai, Ziyi Li, Wendi Li, Xu Wu, Fei Sun, Ping Nie, Yanzhu Luo, Dr. Linlin Li, Ming Zhao, Dr. LinLin Zhang, Dr. Zenan Yu and Dr. Shan Gao. I would also like to thank all my teachers who have helped me to develop the fundamental and essential academic competence.

Last but not least, I would like to thank all my families and friends, especially my boyfriend, Zaiyuan Le, for their encouragement and support.

Table of Contents

Chapter1 Introduction

1.1 Photocatalysis

1.1.1 The principle of photocatalysis

Mimic of natural photosynthesis, the first artificial photosynthesis was reported for water splitting under UV radiation with TiO_2 in 1972 by A.Fujishima and K.Honada.[1] In 1979, the same group reported the photocatalytic CO_2 reduction by different semiconductors.[2] These two discoveries have built up a new era for solar fuel production. After this breakthrough, several studies on photocatalysis have attracted researchers' attention from worldwide.

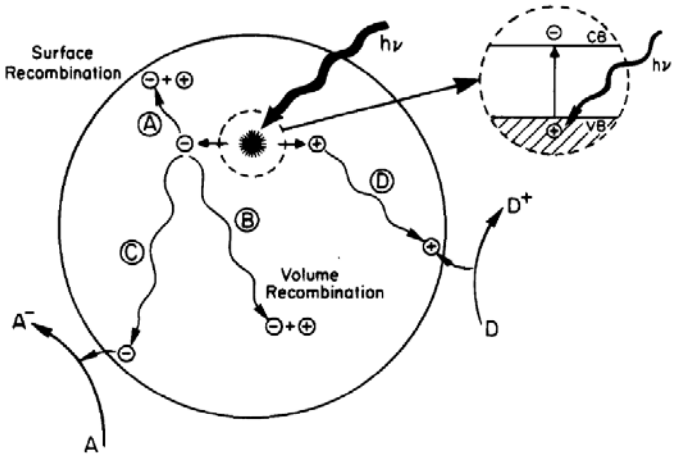

Scheme1. Schematic photoexcitation in a solid followed by de-excitation events.[3]

In general for photochemistry, reaction was happened due to light induced reaction generate charge carriers on photo catalyst surface with the environment. Semiconductors were utilized as photo catalyst due to their unique electronic structure

of filled valence band (VB) and an empty conduction band (CB) meanwhile got superior optical properties. The three fundamental steps were summarized from previous report: 1) Redox equivalents (electron-hole) generated by light absorption. 2) Migration of the redox equivalents to reactive centers. 3) Oxidation and reduction reactions at the catalytic centers.[2]

There are mainly two types of photocatalysis:

a. Homogeneous photocatalysis

In homogeneous photocatalysis, the reactants and the photocatalysts exist in the same phase. The most commonly used homogeneous photocatalysts include ozone and photo-Fenton systems (Fe^{+} and Fe^{+}/H_2O_2). The reactive species is the •OH which is used for different purposes. The mechanism of hydroxyl radical production by ozone can follow two paths.[4]

$O_3 + h\nu \rightarrow O_2 + O(1D)$

$O(1D) + H_2O \rightarrow \bullet OH + \bullet OH$

$O(1D) + H_2O \rightarrow H_2O_2$

$H_2O_2 + h\nu \rightarrow \bullet OH + \bullet OH$

Similarly, the Fenton system produces hydroxyl radicals by the following mechanism[5]

$Fe^{2+} + H_2O_2 \rightarrow HO\bullet + Fe^{3+} + OH^{-}$

$Fe^{3+} + H_2O_2 \rightarrow Fe^{2+} + HO\bullet 2 + H^{+}$

$Fe^{2+} + HO\bullet \rightarrow Fe^{3+} + OH^{-}$

In photo-Fenton type processes, additional sources of OH radicals should be considered:

through photolysis of H_2O_2, and through reduction of Fe^{3+} ions under UV light:

$H_2O_2 + h\nu \rightarrow HO\bullet + HO\bullet$

$Fe^{3+} + H_2O + h\nu \rightarrow Fe^{2+} + HO\bullet + H^+$

The efficiency of Fenton type processes is influenced by several operating parameters like concentration of hydrogen peroxide, pH and intensity of UV. The main advantage of this process is the ability of using sunlight with light sensitivity up to 450 nm, thus avoiding the high costs of UV lamps and electrical energy. These reactions have been proven more efficient than the other photocatalysis but the disadvantages of the process are the low pH values which are required, since iron precipitates at higher pH values and the fact that iron has to be removed after treatment.

b. Heterogeneous photocatalysis

Heterogeneous catalysis has the catalyst in a different phase from the reactants. Heterogeneous photocatalysis is a discipline which includes a large variety of reactions: mild or total oxidations, dehydrogenation, hydrogen transfer and deuterium-alkane isotopic exchange, metal deposition, water detoxification, gaseous pollutant removal, etc.

Most common heterogeneous photocatalysts are transition metal oxides and semiconductors, which have unique characteristics. Unlike the metals which have a continuum of electronic states, semiconductors possess a void energy region where no energy levels are available to promote recombination of an electron and hole produced by photoactivation in the solid. The void region, which extends from the top of the filled

valence band to the bottom of the vacant conduction band, is called the band gap.[3] When a photon with energy is equal to or greater than the materials' band gap, which absorbed by the semiconductor, an electron is excited from the valence band to the conduction band, generating a positive hole in the valence band. The excited electron and hole then recombine and release the energy gained from the excitation of the electron as heat. Recombination is undesirable and leads to an inefficient photocatalyst. The ultimate goal of the process is to have a reaction between the excited electrons with an oxidant to produce a reduced product, and also a reaction between the generated holes with a reductant to produce an oxidized product. Due to the generation of positive holes and electrons, oxidation-reduction reactions take place at the surface of semiconductors. In the oxidative reaction, the positive holes react with the moisture present on the surface and produce a hydroxyl radical.

Oxidative reactions due to photocatalytic effect:

$UV + MO \rightarrow MO\ (h + e^{-})$

Here MO stands for metal oxide ---

$h^{+} + H_2O \rightarrow H^{+} + \bullet OH$

$2\ h^{+} + 2\ H_2O \rightarrow 2\ H^{+} + H_2O_2$

$H_2O_2 \rightarrow HO\bullet + \bullet OH$

The reductive reaction due to photocatalytic effect:

$e^{-} + O_2 \rightarrow \bullet O_2^{-}$

$\bullet O_2^{-} + HO\bullet 2 + H^{+} \rightarrow H_2O_2 + O_2$

$HOOH \rightarrow HO\bullet + \bullet OH$

Ultimately, the hydroxyl radicals are generated in both the reactions. These hydroxyl radicals are very oxidative in nature and non selective with redox potential of (E_0 = +3.06 V)[6]

1.1.2 The application of photocatalysis

Over the last decade, air pollutions in various forms have caused direct or indirect hazards worldwide. So the air pollution control is of grave concern to us all. The use of photocatalysis can effectively remove many toxic substances from the air, such as formaldehyde, acetaldehyde, methanol, acetone, benzene, toluene, methyl mercaptan, dioxins, NOx, CO, SO_2, bacteria,[7-12] relatively harsh conditions required compared to the general heterogeneous catalysis removal method (for examples, require higher temperatures, the potential secondary pollution, complicated steps, etc.), photocatalytic technology to mild reaction conditions, the reaction product green, good product selectivity and operation are simple and the advantages of increasing attention.

1.1.3 Photocatalytic-NOx removal

With the development of economy and industrialization, the air has been polluted and the environment has been destroyed seriously. The major gaseous pollutants include sulfur dioxide (SO_2), carbon monoxide (CO), and nitrogen oxides (NOx) as well as ozone (O_3). Among these major pollutants in waste air, nitrous oxides (NO_x) could

directly or indirectly cause serious harm toward environment and human. These generally include nitrogen monoxide, also known as nitric oxide (NO), and nitrogen dioxide (NO_2). They may also include nitrous oxide (N_2O), nitrogen tetroxide (N_2O_4) and nitrogen pentoxide (N_2O_5).[13] NOx is a regulated pollutant formed in nearly all industrial combustion processes. Thus, the control and removal of NOx in air have become one of the hottest research topics. To date, many actions have been taken to develop and practically apply to remove NOx in the waste gas. The NOx removal can be divided into two groups, primary and secondary methods. The photo de-NOx processes are classified as the secondary method.

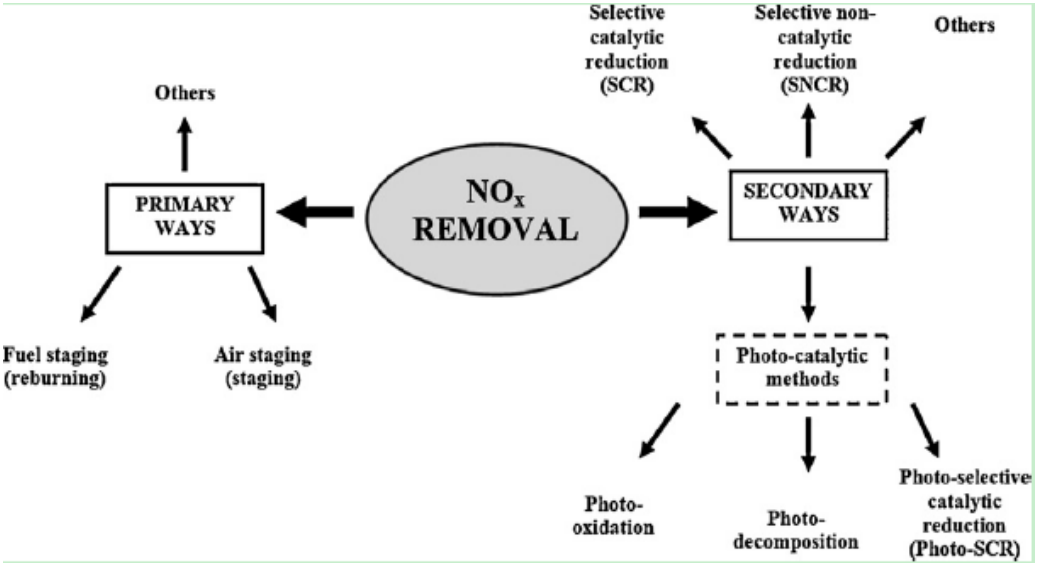

Figure 1. The methods of NOx removal.[13]

However, the primary ways could only remove NOx at high temperature, high concentration and stationary source emissions. it displays poor efficiencies in removing NOx resulted from motor vehicle and trash burning etc. since the NOx in released from those processes generally shows relatively low concentration, long durability, and

difficult purification. Therefore, photocatalysis is an innovative and promising technique to solve the problems. Three ways of de-NOx by photocatalytic reactions are photo selective catalytic reduction, photo-oxidation and photodecomposition.

1.2 Metal organic frameworks materials

MOF are built up from organic linkers and inorganic active centers to form one-, two-, or three-dimensional structures that can be porous, have generated a great deal of interest on the extensive applications for potential applications in analytical areas, including adsorption[14, 15], catalysis[16], H_2[17] or CO_2[18] storage, separation[19-21], and chemical sensors[22, 23], due to the merits such as large surface areas, large pore volumes, diverse functionalization of pore, and functionalization of diversification. Traditionally, the overriding goal of MOF synthesis has been to obtain high quality single crystals for structural analysis. In Fig.1, it shows the scheme of different kind of MOFs.

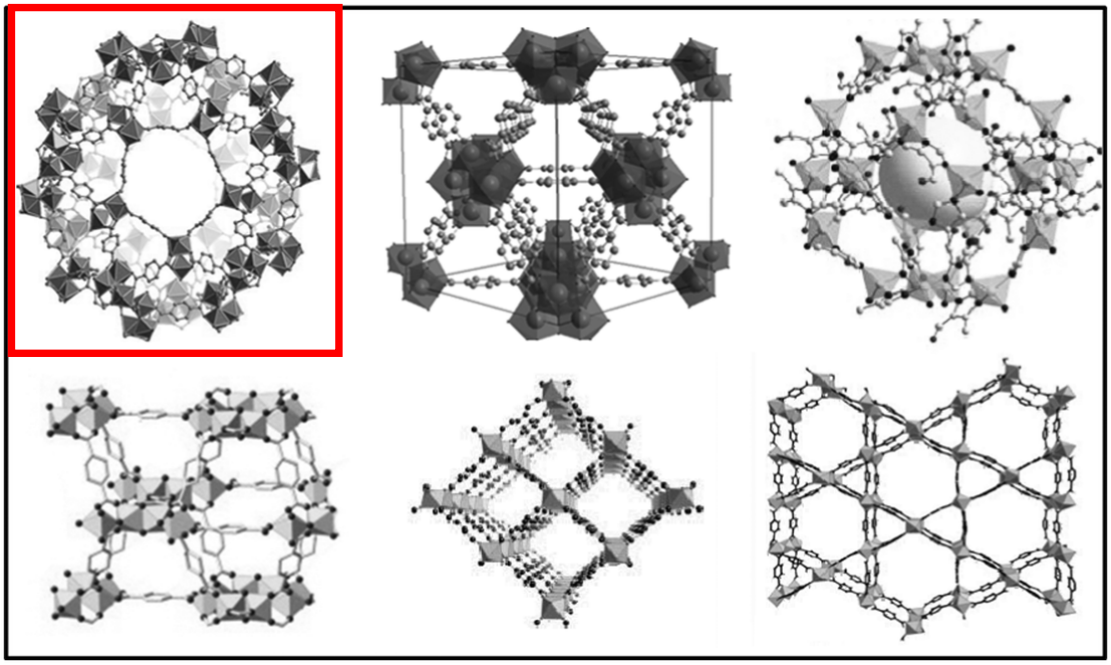

Figure 2. The Scheme of pore topologies for the different MOFs. Upper line, from left to right, MIL-125, UiO-66, SIM-1. Bottom line, from left to right, MIL-125, MIL-53, MIL-68.[24]

Among the wide variety properties of interest, several MOFs exhibit very interesting PEC features. For example, MOF-5 and ZnO@ZIF-8 nanorods have been successfully used in these PEC sensors.[25] Among them, (Ti) NH2-MIL-125(Ti) (MIL-125), as an amino functionalized titanium (IV) the MOF material, exhibited special photo or catalytic properties, such as photochromic behavior[26], photocatalytic reduction of water to hydrogen gas[27], and desulfurization[28]. Recently, more explorations on the application of MIL-125 (Ti) have been extended to photoelectrocatalytic detection of herbicide clethodim through an amino functionalization with the formation of NH_2-MIL-125 (Ti) owing to the inclusion of amine moieties and the extended absorption

spectra into visible-light region[29].

Nevertheless, NH_2-MIL-125 (Ti), as a photocatalyst, still suffers from the fast recombination of photogenerated electrons and the cluster-centers (Ti), resulting poor photocatalytic/photoelectrocatalytic performance for the further utilization in both environmental remediation and energy production based on reduction of protons. Thus, it is highly required for searching an effective way to inhibiting the electron-hole recombination while keeping the nature photo-response property of NH_2-MIL-125 (Ti) unchanged.

1.3 Microwave assisted synthesis

Microwaves are a portion of the electromagnetic spectrum with frequencies in the range of 300 MHz to 300 GHz. The commonly used frequency is 2.45 GHz. Molecules with a permanent dipole moment can align themselves through rotation completely or at least partly with the direction of the field. For countless polar substances, dielectric losses are observed in the microwave range. A simplified illustration of the heating mechanism of polar solvents by microwave radiation is provided in Scheme 2 for the case of H_2O.

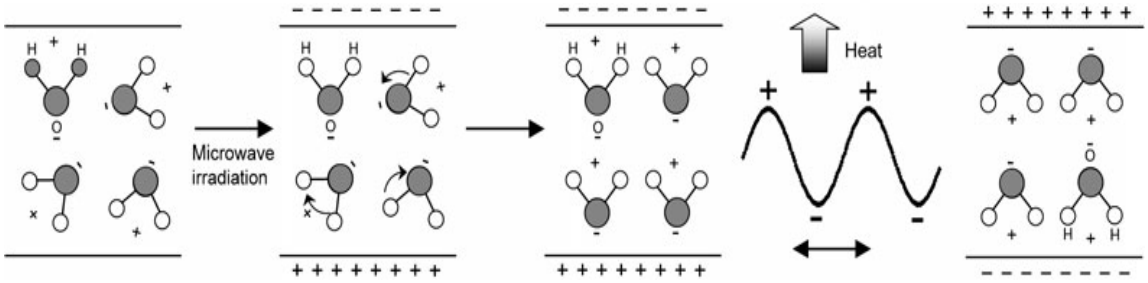

Scheme 2. Heating mechanism of H2O by microwave irradiation.[30]

The fast changing electric field of the microwave radiation leads to a rotation of the water molecules. Due to this process, “internal friction” takes place in the polar medium, which leads to a direct and almost even heating of the reaction mixture. Because the change in the polarity of the electric field is faster than the rotation of the water molecules around its dipole center, a phase shift results and energy is absorbed from the electric field. Reflections and refractions on local boundaries yield “hot spots” and may result in a “super-heating” effect, which has been controversially discussed in the literature.[31, 32]

	B.p. [°C]	ε'	ε''	$\tan\delta$
water	100	78.3	12.3	0.157
methanol	65	32.7	20.9	0.639
ethanol	78	24.3	6.08	0.200
N,*N*-dimethyl formamide (DMF)	153	36.71	–	–
ethylene glycol (EG)	198	41.0	41.0	1.00
N-methyl pyrrolidone (NMP)	202	32.0	8.855	0.277

Table 1. Physical parameters of typical solvents used for microwave heating[33]

The physical parameters of typical solvents used in MW heating for synthesis of metallic nanostructures are listed in Table 1. Water, alcohols, DMF, and ethyleneglycol (EG) have high dielectric losses and a high reduction ability. Therefore, they are ideal solvents for MW rapid heating.

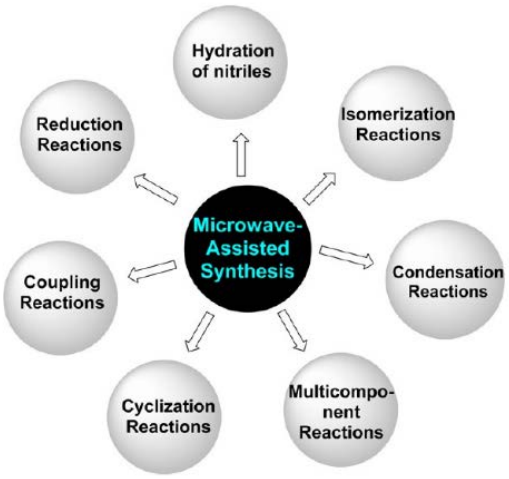

Figure 3. Applications of microwave-assisted synthesis.

Microwave-assisted synthesis fulfills the promise of being a fast synthesis practice. Since the first reports in 1986,[34, 35] the use of the Microwave heating technique has become an essential tool in all areas of synthetic organic chemistry, including solvent-free and water-mediated reactions (Figure 5).[36-40] Lately, it has been postulated that the synthesis of nanomaterials, metal nanoparticles, and nanostructures, whose growth is highly sensitive to the reaction conditions, could benefit a great deal from the efficient and controlled heating provided by Microwave irradiation. The use of nanomaterials and magnetically recyclable catalysts in organic synthesis under benign aqueous reaction conditions is becoming increasingly popular.[41, 42]

1.4 Graphene Oxide

Graphite oxide (GO), also known as graphitic oxide or graphitic acid, is a compound of carbon, oxygen, and hydrogen in variable ratios, obtained by treating graphite with strong oxidizers. Gaphene oxide is its easy dispersability in water and other organic solvents, due to the presence of the oxygen functionalities.

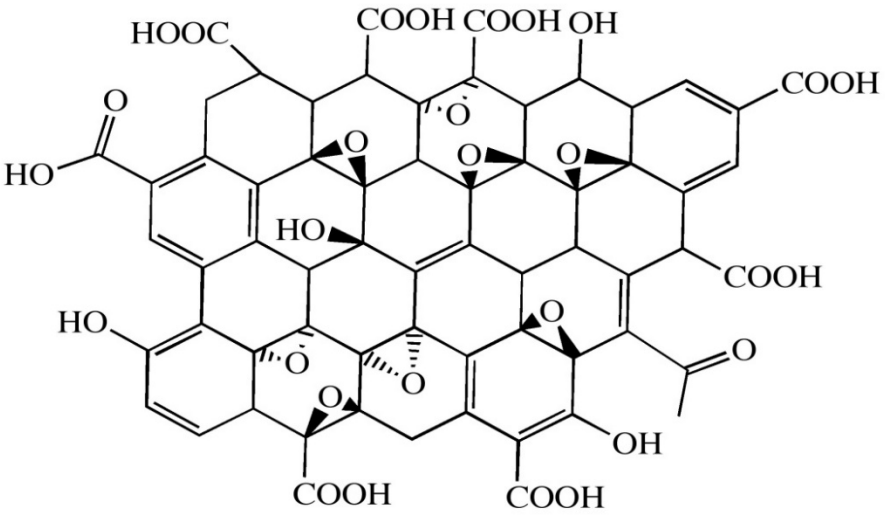

Figure 4. Scheme of Graphene Oxide

It is lucky that the graphene oxide has been proved as the conductive carbon materials for effectively improving the semiconductor optical catalyst performance via accelerating the electron-transfer[43, 44].

Meanwhile, GO, as an alternative of soft carbon material, also possesses the various characteristics of colloids, polymer films, as well as the amphoteric molecules, allowing it to contain rich functional groups, such as epoxy groups and hydroxyl groups. These groups on GO may serve as the nucleations for the fabrication of NH_2-MIL-125(Ti), ensuring a good dispersion of the as-obtained MOF crystals on the surface of GO. Considering that GO is also an excellent microwave absorbing materials owing to its

high permittivity[45]. Even under 1Hz irradiation, its dielectric constants still can be maintained about 689.[46] Thus, it is reasonable that GO could serve as an antenna for absorbing microwave with the formation hot spots on the surface of GO, supplying a suitable and benign thermal condition for the growth of NH_2-MIL-125(Ti) with a high crystallinity[47, 48].

In the present work, a microwave-induced fast route was proposed for the *in-situ* fabrication of NH_2-MIL-125(Ti) loaded on GO nanosheets substrates. By using such a route, monodispersed NH_2-MIL-125(Ti) with high crystallinity were closely bonded to the surface of GO. The aggregation of NH_2-MIL-125(Ti) was effectively prevented in the presence of GO matrix, allowing the MOF particles dispersed on GO layers. Such GO/NH_2-MIL-125(Ti) composites exhibited an obviously enhanced photocatalytic activity for treating the gaseous pollutants (NO_x and acetaldehyde) compared to the pure NH_2-MIL-125(Ti) owing to the greatly enhanced visible-light adsorption capability, photocurrent intensity, electron carrier density, strong heterojunctions, and low electron-hole recombination rates.

Chapter 2 Experimental Method

2.1 Materials and Reagents

2-Aminoterephthalic acid (H_2ATA) were purchased from Sigma-Aldrich. Titanium isopropoxide ($C_{12}H_{28}O_4Ti$), dimethylformamide (DMF), and ethanol were purchased from Aladdin. These reagents were analytical grade and used without further purifications. Graphene oxide was prepared *via* a Hummers method.[49]

2.2 The preparation of GO/NH_2-MIL-125 (Ti)

In a typical synthesis process, 1.0 g H_2ATA and 10.0 mg as-obtained GO were dispersed into a mixture solution containing 18.0 mL DMF and 3.0 mL methanol with strong stirring under ultrasound (Ultrasonication cleaner, 180 W, DS-3510DTH, Shanghai) at room temperature for 90 min. Then, 100 uL $C_{12}H_{28}O_4Ti$ was added into the above mixture, while keeping stirring and ultrasonication for 10 min. The as-obtained mixture solution was further sealed in a 50 mL Teflon lined double-walled digestion vessel. After treating at 150 °C for 30 min using a microwave digestion system (Ethos TC, Milestone), the vessel was then cooled down to room temperature. The resulted suspension was centrifuged and washed with DMF and methanol, respectively. The as-obtained powders were further dried in air at 60 ^oC for achieving the final solid product (denoted as X-GO/NH_2-MIL-125 (Ti), X means the weight value in a unit of mg, X = 5, 10, 15, 20, and 25). For comparison, pure NH_2-MIL-125(Ti) was also synthesized by the same route in the absence of GO. Mechanical mixing samples were also prepared

by mixing the 10 mg GO and the as-prepared NH_2-MIL-125(Ti) *via* grinding in air at room temperature. It was denoted as M10-GO/NH_2-MIL-125 (Ti).

2.3 Characterization

The morphology was observed via field emission scanning electron microscopy (FESEM, HITACHI S-4800) and transmission electronic micrograph (TEM, JEOL JEM-2100). UV-vis diffuse reflectance spectra (DRS) were obtained on a UV-vis spectra photometer (DRS, UV-2450). The Brunauer–Emmett–Teller (BET) approach was used to determine the surface area. X-ray photoelectron spectroscopy (XPS) was done on a PerkinElmer PHI 5000C ESCA system to analyze electronic states. All the binding energies were calibrated by using the contaminant carbon (C1S = 284.6 eV) as a reference. The Fourier transformation infra-red spectrum (FTIR) experiments were carried out on an AVATAR 370 FT-IR spectrometer. The photoluminescence spectroscopy (PLS) was collected on Varian Cary-Eclipes 500 with an excitation light at 264 nm.

2.4 Photoelectrochemical (PEC) measurements

Photoelectrochemical measurements were performed in a three-electrode, single-compartment quartz cell on an electrochemical station (CHI 660D). The GO and GO/NH_2-MIL-125 (Ti) electrodes (active area of 4 cm^2, coated on ITO glass) were

utilized as the working electrodes. A platinum sheet (99.99%, 0.1 mm, 2 cm*2 cm) and saturated calomel electrode (SCE) were used as the counter electrode and reference electrode, respectively. A 300 W Xenon lamp ($\lambda > 420$ nm, with an ultraviolet filter), as the visible-light source, was positioned 10 cm away from the photoelectrochemical cell. Impedance measurements were performed under visible light illumination ($\lambda > 420$ nm) in a 0.5 mol/L Na_2SO_4 solution at open circuit voltage over a frequency range from 10^5 to 10^{-1} Hz with an AC voltage at 5 mV. The transient photocurrent was measured using a 20 s on-off cycle at a bias voltage of 0.5 V. The Mott-Schottky plots were obtained at a fixed frequency of 1 KHz to determine the flat-band potential and carrier density.

2.5 Activity test

The photocatalytic NO oxidation in gas phase was carried out at ambient temperature in a continuous flow reactor with volume of 4.5 L (10 × 30 × 15 cm). During visible light driven photocatalysis, 2*150 W tungsten halogen lamps (General Electric) located vertically above the reactor by cutting the lights with wavelength shorter than 420 nm using an ultraviolet filter.[50] In each test, an air gas flow containing 500 ppb NO was pumped through 0.10 g photocatalyst (coated onto a glass dish with a diameter of 15.0 cm) at the rate of 4.0 L/min. The desired humidity level of the NO flow was controlled at 70 % (2100 ppmv) by passing the zero air streams through a humidification chamber. After reaching adsorption-desorption equilibrium on the photocatalyst, the lamp was

turned on to start the photocatalysis reaction. The concentration of NO was continuously measured by using a chemiluminescence NO analyzer (Thermo Environmental Instruments Inc. Model 42i). The NO removal rate (%) was calculated based on the following equation: NO removal rate (%) = $(C_0 - C)/C_0 \times 100\%$, where C_0 and C refer to the NO concentration determined before and after reaction.[51]

The photocatalytic oxidation of gaseous acetaldehyde was carried out in a self-designed stainless steel reactor with a quartz glass window at 25 ^oC. In a typical test, 50.0 mg photocatalyst was dispersed in 10 mL anhydrous ethanol in a watch glass under ultrasonication for 0.5 minutes, and dried at 80 ^oC for 15 min. The dried watch glass contained samples was transferred into the above reactor. Then, 5.0 uL acetaldehyde was rapidly injected the reactor with the formation of the simulated organic gas pollutant ($[CH_3CHO]$ = 1.95 mg/L, after reaching the absorption-desorption equation). A 300 W Xenon lamp, with a 420 nm cutoff filter, was used as a visible-light source for driving the photo-oxidation reaction. The distance between the reactor and Xenon lamp is 15 cm. Each photocatalytic oxidation reaction was performed for 60 min, and the remained gas was sampled and analyzed using a gas chromatograph (Shimadzu, GC-17A) for determining the final concentration of acetaldehyde.

Chapter 3 Results and discussion

The morphologies of GO, NH_2-MIL-125(Ti) and GO/NH_2-MIL-125(Ti)

nanocomposites were analyzed by scanning electron microscope (SEM). As shown in Fig. 1a, the GO samples possessed a regular fold structure. The NH_2-MIL-125(Ti) was composed of aggregated flat spherical grains, with an average size of about 200 nm, as shown in Fig.1b. Such aggregation could be well avoided by introducing GO. From Fig. 1c, highly dispersed grains were observed on the surface of GO. Moreover, the size of the NH_2-MIL-125(Ti) loaded on GO was lower than that of pure NH_2-MIL-125(Ti) sample.

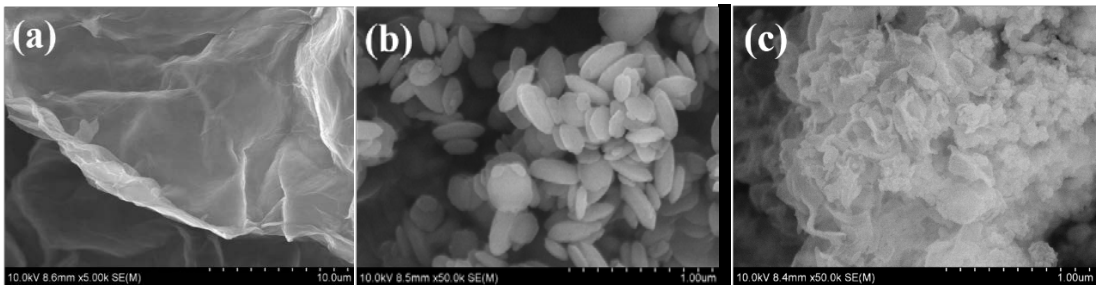

Figure 5. FESEM image of (a) GO, (b) NH_2-MIL-125(Ti) and (c) 10-GO/NH_2-MIL-125(Ti)

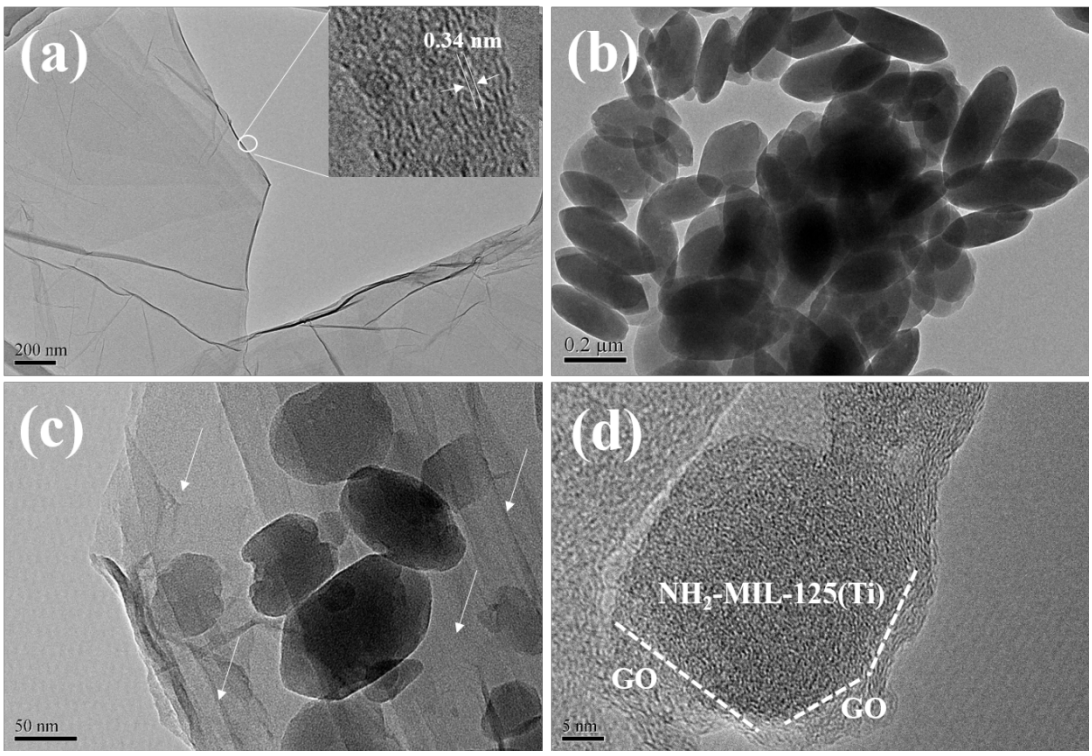

Figure 6. TEM image and HRTEM (inset) of GO (a), NH_2-MIL-125(Ti) (b), and 10-GO/NH_2-MIL-125(Ti) (c, d).

The transmission electron microscopy (TEM) images of GO (Fig. 2a) support the assertion that the as-prepared GO exhibited a regular fold structure with a few layers thickness, suggested by the inset of Fig.2a. Such appearance of fold structure is mainly due to oxidation process, which was introduced to the sp^2 hybrid carbon atoms in the sp^3 hybridization of carbon atoms.[49] Two-dimensional plane of GO layer structure could be distorted by some carbon atoms connected with -OH groups, with the formation of fold of lamella. Flat spherical NH_2-MIL-125(Ti) crystals were obtained *via* the microwave thermal process, as shown in Fig. 2b, however, they still suffered a serious aggregation. It was interesting that these metal organic framework (MOF) crystals could be highly dispersed on the surface of GO (highlighted by white arrows)

upon introducing GO nanosheets into the microwave solvothermal process, as shown in Fig. 2c. Compare to that of NH_2-MIL-125(Ti), the 10-GO/NH_2-MIL-125(Ti) sample possessed a smaller grain size of NH_2-MIL-125(Ti), probably because of the grain refinement in the microwave reaction process. This could be attributed to that the GO nanosheets could serve as an antenna for absorbing microwave with the formation hot spots on the surface of GO ("hot-spots effect"), supplying a suitable and benign thermal condition for the growth NH_2-MIL-125(Ti). The high resolution images of 10-GO/NH_2-MIL-125(Ti), as shown in Fig. 2d, explicitly differenciated the GO skeleton from the NH_2-MIL-125(Ti) crystals. This also clearly indicated that strong interations (heterojunctions) existed on the interface between GO and NH_2-MIL-125(Ti) owing to the hot-spots effect. Such heterojunctions would be favorable for enhancing the photocatalytic performance of NH_2-MIL-125(Ti).

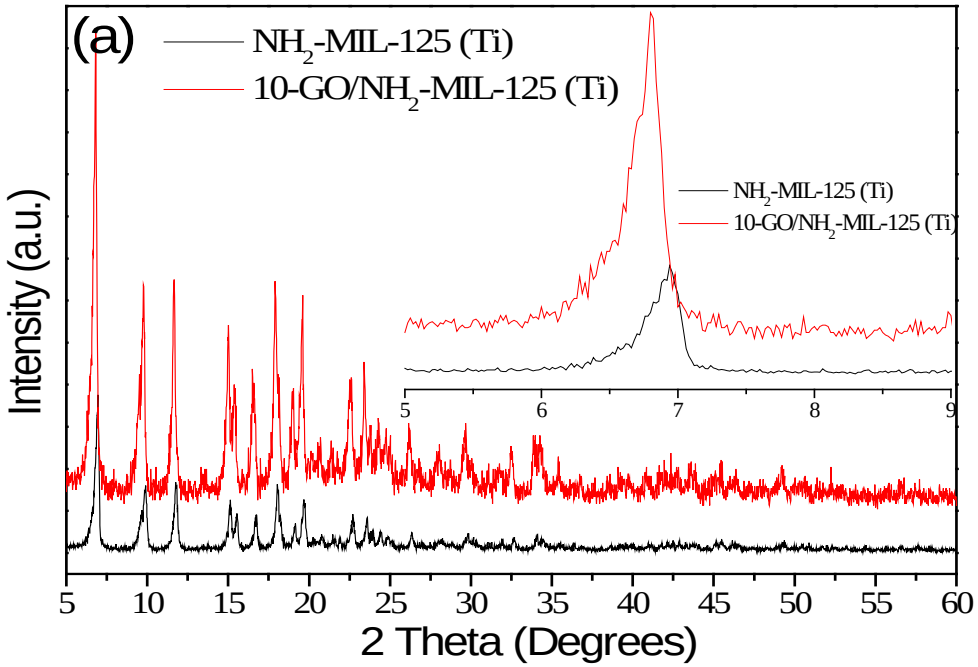

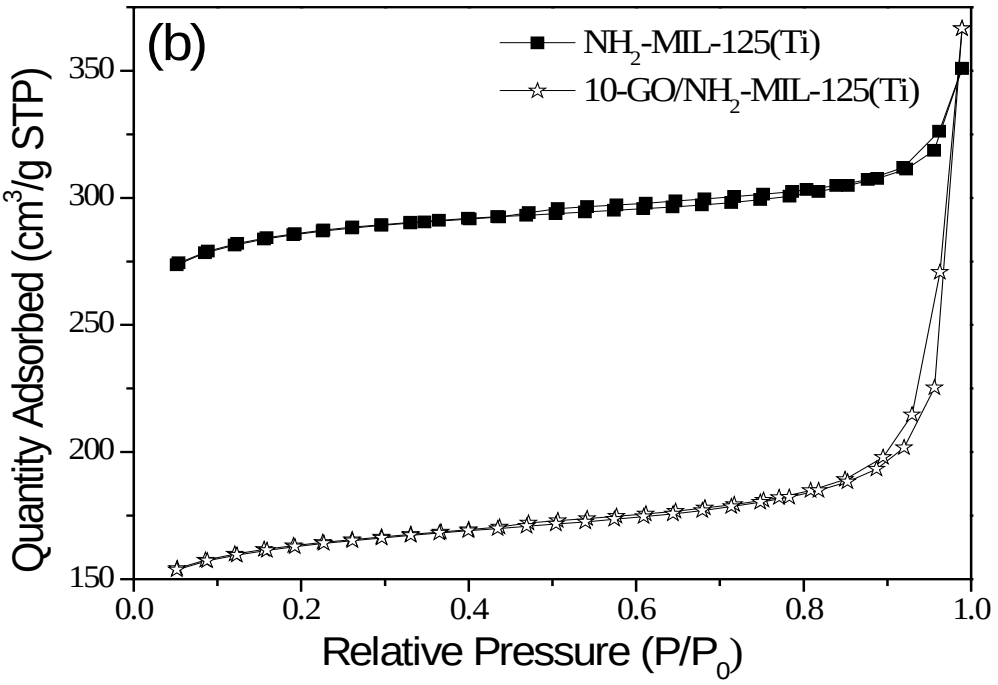

Figure 7. The XRD patterns (a) and the N_2 adsorption-desorption isotherms (b) of NH_2-MIL-125(Ti) and 10-GO/NH_2-MIL-125(Ti).

For illustrating the crystal structure and morphology of the as-obtained pure and GO grafted NH_2-MIL-125(Ti) samples, X-ray diffraction (XRD) was recorded as shown in Fig. 3a. Both of the two samples possessed the typical diffraction peaks of NH_2-MIL-125(Ti),[26, 52] suggesting the formation of perfect NH_2-MIL-125(Ti) crystals on GO under the microwave solvothermal process. Nevertheless, it should be pointed out that the intensity of the main diffraction peak of 10-GO/ NH_2-MIL-125(Ti) was much higher than that of the pure NH_2-MIL-125(Ti). This illustrated that greatly improved crystallinity of NH_2-MIL-125(Ti) could be produced in the presence of GO under microwave irradiation, probably because of the “hot-spots effect” of GO in microwave solvothermal process, allowing a better crystallization of NH_2-MIL-125(Ti). Moreover, it was also observed from the enlarged XRD pattern (the inset of Fig. 3) that the

diffraction peaks of 10-GO/ NH_2-MIL-125(Ti) shifted to a lower angle compared to that of pure NH_2-MIL-125(Ti). Thus, it is reasonable that strong interactions were formed between GO and NH_2-MIL-125(Ti) in the GO/NH_2-MIL-125(Ti) composites. The nitrogen adsoprtion-desorption isotherms were also obtained at 77 K for investigating the textural properties of the GO/NH_2-MIL-125(Ti) hybrids as shown in Fig. 3b. A typical type I adsorption isotherm was observed for the sample of pure NH_2-MIL-125(Ti) with a Langmuir surface area of ca. 871 m^2/g, indicating zeolite/zeolite-like crystalline solids were obtained in the present work according to the IUPAC classification.[53] Such MOF microstructure could be well maintained even after introducing GO under microwave-irradiation because 10-GO/NH_2-MIL-125(Ti) still possesses a type I adsorption isotherm shape, though a lower Langmuir surface area 502 m^2/g was produced. Such high surface area could play an important role in both enhancing the light absorption capability and supplying an enough high active sites for driving the photocatalytic reactions.[54]

For further detecting the composition of the as-obtained materials, the Fourier transform infrared spectroscopy (FTIR) spectra of GO, NH_2-MIL-125(Ti) and 10-GO/NH_2-MIL-125(Ti) in the region of 450-4000 cm^{-1} measured at room temperature were shown in Fig. 4a. The spectrum of the as-obtained GO (black trace) presented the characteristic bands of O-H stretching vibrations (3420 cm^{-1}), C=O stretching vibration (1740 cm^{-1}), C=C from un-oxidized sp^2 CC bonds (1620 cm^{-1}), C-OH vibration (1400 cm^{-1}) and C-O-C vibrations (1080 cm^{-1}).[43, 55] Such vibration absorption peaks indicated

that that regular oxidized graphene phase was achieved. The FTIR spectra of NH_2-MIL-125(Ti) exhibited the characteristics of the stretching vibrations of the hydroxyl at 3450 cm^{-1}, the amino at 3350 cm^{-1}, the carboxylate in 1380-1600 cm^{-1}, and (O-Ti-O) vibrations in 400-800 cm^{-1}.[56]

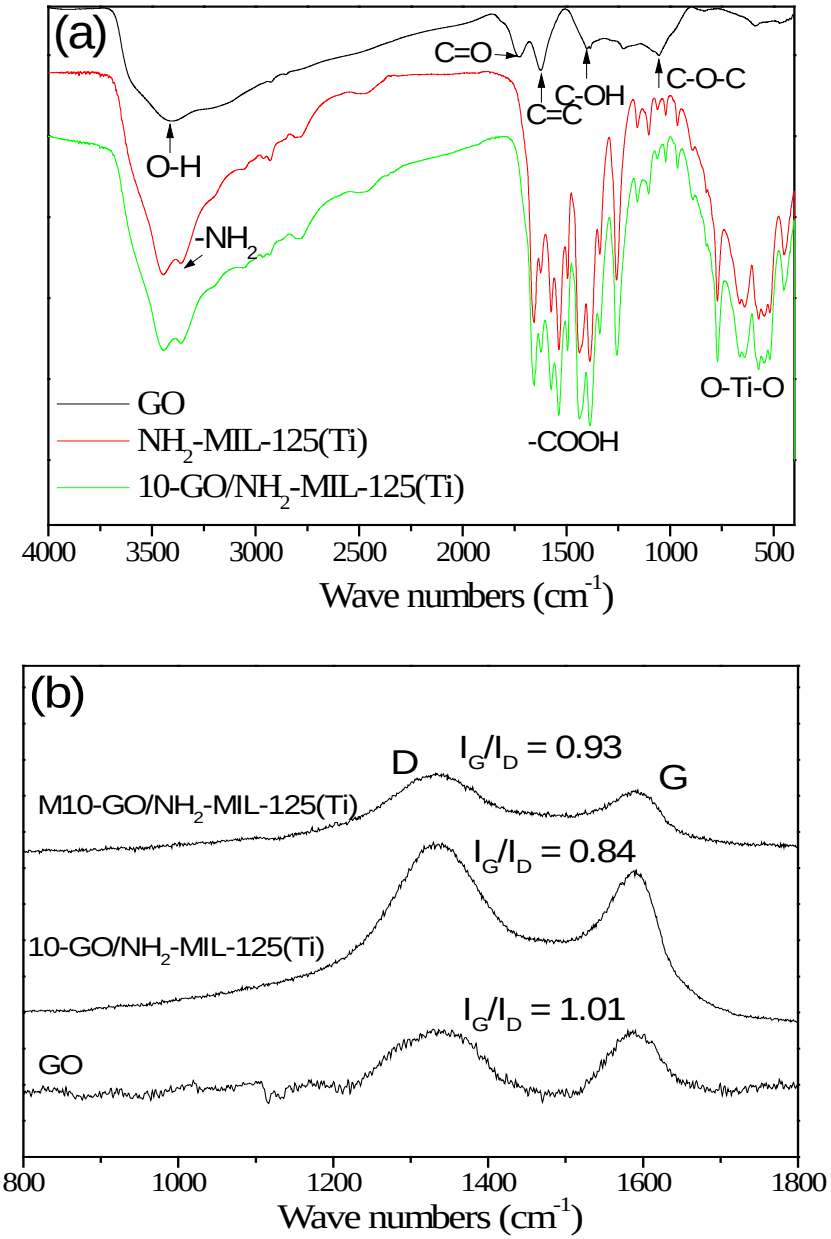

Figure 8. (a) FTIR spectra of GO, NH_2-MIL-125(Ti) and 10-GO/NH_2-MIL-125(Ti) and (b) Raman spectra of GO, 10-GO/NH_2-MIL-125 (Ti), and M10-GO/ NH_2-MIL-125 (Ti).

The carboxylate stretching vibrations can be defined doublet bands (at 1530 and 1430 cm^{-1}), assigned to the COO- antisymmetric and symmetric stretching vibrations complexed with surface Ti centers.[43, 57] Upon being combined with GO, the FTIR spectrum of 10-GO/NH_2-MIL-125(Ti) exhibited a strong doublet bands of the COO^- antisymmetric and symmetric stretching vibrations, indicating that NH_2-MIL-125(Ti) crystals were closed bonded with GO through carboxylates. As known, Raman spectroscopy has been proved effective for the investigation and detailed characterization of graphitic materials for achieving various important information, including crystallite size, clustering of the sp^2 phase, the presence of sp^2-sp^3 hybridization, the introduction of chemical impurities and so on.[58] Thus, it was utilized to analyze the similarities and differences between GO and 10-GO/NH_2-MIL-125 (Ti) composites. As shown Fig. 4b, all of the samples exhibited the D bands at ca. 1310 cm^{-1} (disorder-induced vibrational mode) and the G bands at ca. 1600 cm^{-1} (the E2g vibration mode of the sp^2-bonded graphitic carbons). It was noted that the intensity ratio of G band to D band (the I_G/I_D ratio, indicative of the degree of structural defects and a quantitative measurement of edge plane exposure)[58, 59] was decreased from 1.01 to 0.84 upon growing NH_2-MIL-125 (Ti) crystals on the surface of GO under microwave solvothermal process. This could indicate that the GO was partly reduced into graphene by NH_2-MIL-125 (Ti) in the microwave solvothermal conditions. It should be pointed out that the mechanical mixing sample of M10-GO/ NH_2-MIL-125 (Ti) exhibited a higher I_G/I_D ratio (0.93), compared to 10-GO/NH_2-MIL-125 (Ti). Such difference of

I_G/I_D ratio could be attributed to the interactions strength between GO and NH_2-MIL-125 (Ti). These results suggested that a strong interaction was produced in microwave solvothermal process between GO and NH_2-MIL-125 (Ti), with the formation of heterojunctions probably facilitating the electron transfer from NH_2-MIL-125 (Ti) to GO.

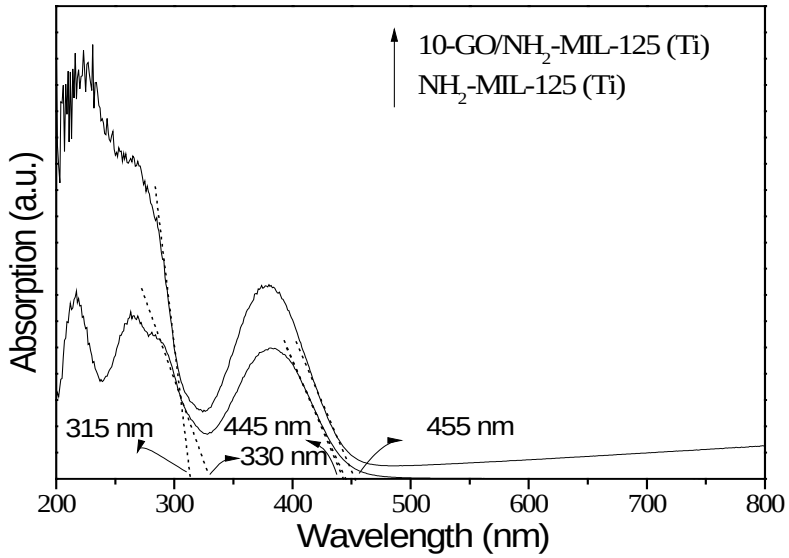

Figure 9. UV-Vis DRS spectra of NH_2-MIL-125(Ti) and 10-GO/NH_2-MIL-125(Ti).

The UV/vis diffuse reflectance spectra (DRS) is strong tool for evaluating the electronic state and photo-absorption capability of the photoactive materials.[54] Thus, we further used DRS to investigate the promotion effect of GO on the NH_2-MIL-125(Ti) crystals. As shown in Fig. 5, the as-formed NH_2-MIL-125(Ti) has two significant absorption below 500 nm. The absorption band edges at about 330 nm (band gap energy of 3.76 eV) and 445 nm (bang gap energy of 2.79 eV) were corresponding to the absorption of Ti-O oxo-clusters and the ligand-based absorption, respectively.[60] Upon being grafting on the surface of GO *via* a microwave

solvothermal process, the absorption intensity of 10-GO/NH_2-MIL-125(Ti) in the range of 200-500 nm was greatly increased, indicating the introduction of GO may alter the background absorption into broad light region and improve the utilization of solar energy.[61, 62] It was also noted that the absorption edge of Ti-O oxo-clusters shifted from 330 nm to about 315 nm, and the absorption edge of ligands shifted from 445 nm to 455 nm. The former (blue shift) could be attributed to the interaction between the carboxylates on GO and the Ti centers in NH_2-MIL-125(Ti). The later (red shift) indicated that the strong interaction between GO and NH_2-MIL-125(Ti) could alter the optical property of the ligands, with an extended light absorption region. Thus, less energy of light can drive the as-prepared materials for photocatalytic reaction.

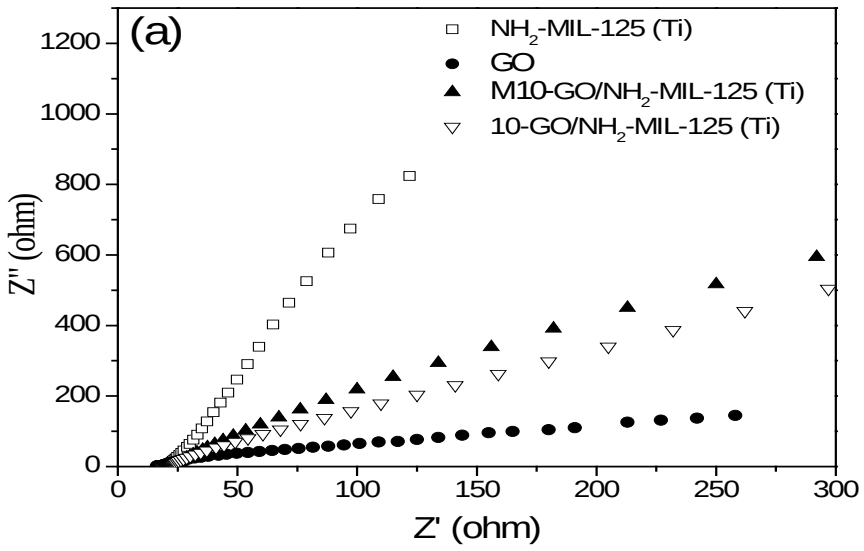

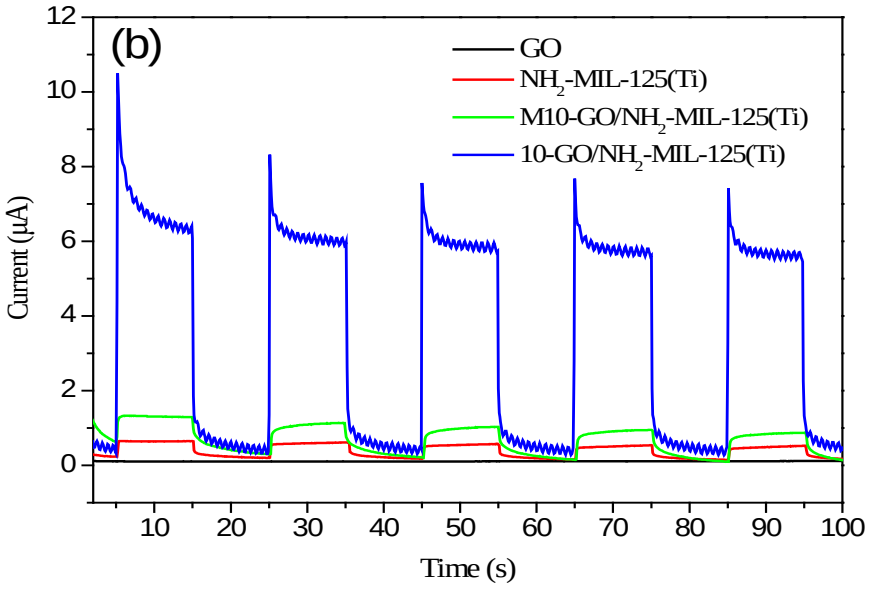

Figure 10. (a) EIS Nynquist plots at open circuit potential, the x axis and y axis represent the real part of the impedance (Z′) and the imaginary part of the impedance (Z″), respectively and (b) photo-current responses in the light on-off process (0.5 V vs. SCE) of various samples. All of the experiments performed using a 300 W Xe lamp irradiation ($\lambda > 420$ nm), with 3-electrode cell, immersed in a 0.5 M aqueous Na_2SO_4 electrolyte using Pt as counter electrode and saturated calomel electrode as reference electrode.

For better clarifying the promotion effect of GO on the photo-electronic property of the as-obtained samples, both electrochemical impedances spectroscopy (EIS) and photo-current response were evaluated by coating these samples on ITO glass. As known, charge-transfer process of the electrode can be illustrated by the semicircle in the Nyquist plot at high frequency, and the diameter of the semicircle may reflect the charge-transfer resistance. As shown in Fig. 6a, GO possessed the smallest arch owing to its excellent conductivity.[63] NH_2-MIL-125(Ti) exhibited the largest arch, however,

such arch value could be greatly decreased after introducing GO, implying that decoration with GO may significantly enhance the electron mobility by reducing the recombination of electron-hole pairs. As shown in Fig. 6b, the photocurrent density of 10-GO/NH_2-MIL-125(Ti) about 13 times of that of NH_2-MIL-125(Ti) under visible light (λ > 420 nm) irradiation, probably owing to the increased of light trapping capability and effective reduction of electron-hole pairs recombination rate. From Fig. 6a and b, one can found that the mechanical mixing sample (M10-GO/NH_2-MIL-125(Ti)) exhibited lower conductivey and photo-current compared to 10-GO/NH_2-MIL-125(Ti). This further supported that the effective combination of GO and NH_2-MIL-125(Ti) may greatly promote the separation of electron-hole pairs through the heterojunctions.

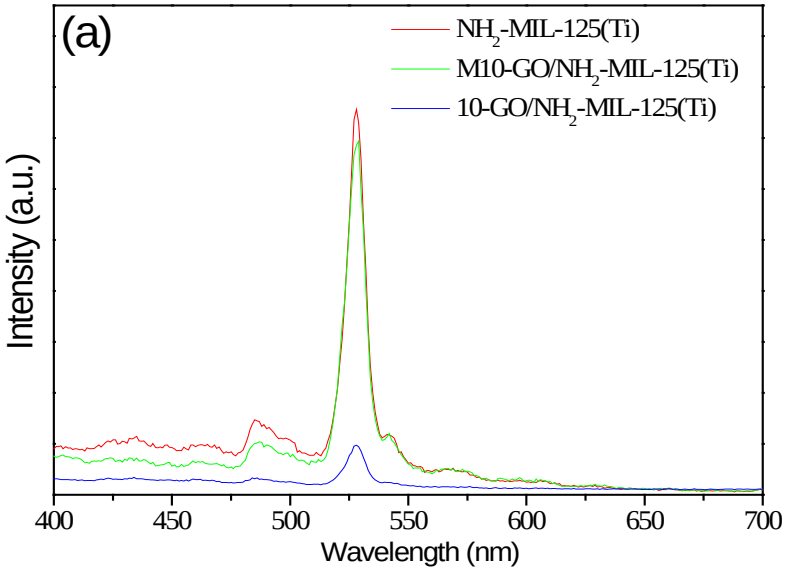

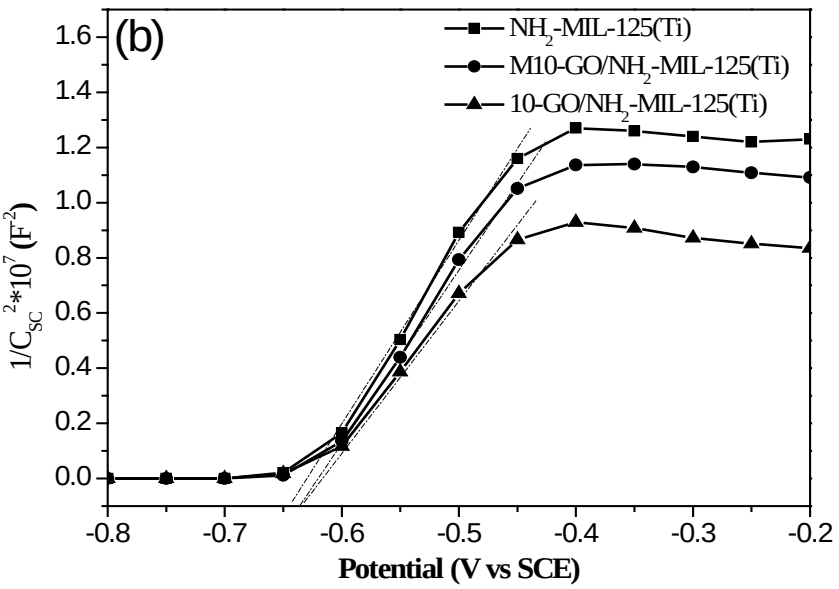

Figure 11. Photoluminescence (PL) spectra (a) excited by 264 nm and Mott-Schottky plots obtained under visible-light irradiation (λ = 420 nm) of NH_2-MIL-125(Ti), 10-GO/NH_2-MIL-125(Ti) and M10-GO/NH_2-MIL-125(Ti).

It is known that the PL signals of photo-responsible materials results from the recombination of photo-induced charge carriers. Thus, PL was proved as an effective technology for evaluating the performance of the photo-generated charge carrier trapping, migration, and transfer.[64] Generally, the exhibited lower PL intensity under light irradiation may suggest the lower recombination rate of photo-generated electron-hole pairs.[65, 66] The pure NH_2-MIL-125(Ti) sample displays a PL peak at around 528 nm, as shown in Fig. 7a. Such peak was greatly weakened upon being combined with GO via microwave solvothermal treatment, indicating that the formation of GO/ NH_2-MIL-125(Ti) hybrids could significantly prohibit the photo-generated charge carrier recombination. The interaction between GO and NH_2-MIL-125(Ti) can create a new way to extend the service life of electronic-hole via facilitating the electron transfer

through GO. Electron cannot return from excited state to ground state, thus directly weakens the photoluminescence intensity of NH_2-MIL-125(Ti). We also noted that the mechanical mixing sample, M10-GO/NH_2-MIL-125(Ti), exhibites a much higher PL intensity than 10-GO/NH_2-MIL-125(Ti) prepared via the microwave process. This could be asscribed to the weak interaction between GO and NH_2-MIL-125(Ti) *via* grinding. Electrons cannot be well transfered through such weak interaction. This phenomenon related to the weak interaction-to-strong PL intensity was also proved by our previous reports.[64] For better comparing the electron carrier density (N_D) order of the as-obtained samples, Mott-Schottky plots were performed under visible-light irradiation ($\lambda > 420$ nm) as shown in Fig. 7b. Based on the Mott-Schottky equation: $N_D = \frac{2C^2}{e\varepsilon\varepsilon_0}(E - E_{FB} - \frac{KT}{e})$, where C is the space charge capacitance in the semiconductor, N_D is the electron carrier density, e is the elemental charge value, ε_0 is the permittivity of a vacuum, ε is the relative permittivity of the semiconductor, E is the applied potential, E_{FB} is the flat band potential, T is temperature, and k is the Boltzmann constant, it is reasonable that the N_D value of various samples was inversely proportional versus the slope of the tangent (dot lines in Fig. 7b) of Mott-Schottky plots. The slopes of NH_2-MIL-125(Ti), M10-GO/NH_2-MIL-125(Ti), and 10-GO/NH_2-MIL-125(Ti) are $6.6656*10^7$, $6.2622*10^7$, and $5.5266*10^7$, respectively. Based on the above results, the ratio of N_D for various samples in the same order was calculated to be about 1: 1.064: 1.206. Such results proved that the strong interaction between GO and NH_2-MIL-125(Ti) could greatly enhance the electron carrier density, thus, 10-GO/NH_2-MIL-125(Ti) could serve as an excellent photocatalyst for driving catalytic process owing to

its high electron transfer capability.

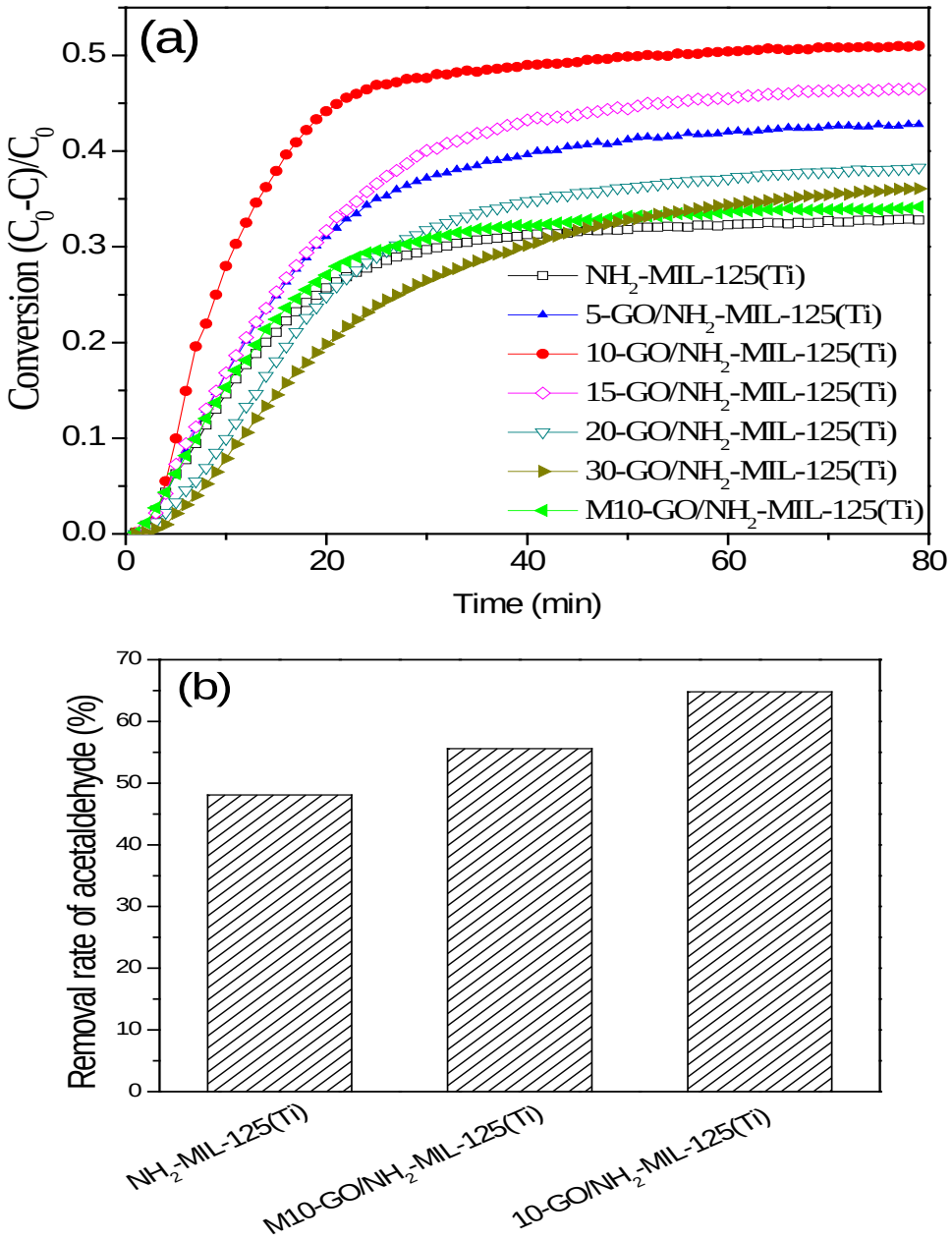

Figure 12. (a) The photo-oxidation of NO under visible-light (λ > 420 nm, 300 W tungsten lamp) irradiation; (b) the photo-degradation of gaseous acetaldehyde under visible-light irradiation (λ > 420 nm, 300 W xenon lamp) in the presence of 50.0 mg catalyst, the initial [CH_3CHO] = 1.95 mg/L.

For evaluating the photocatalytic activity of the NH_2-MIL-125(Ti) based photocatalysts,

the photooxidation of NO in a flow reactor was performed under visible light irradiation. As shown in Fig. 8a, the pure NH_2-MIL-125(Ti) sample exhibited a ca. 30 % NO removal rate after about 30 min. Such value could be well maintained for continously treating NO, suggesting NH_2-MIL-125(Ti) is a durable photocatalyst for oxidation NO under light irradiation. Upon introducing GO for loading NH_2-MIL-125(Ti), the photocatalytic activity was greatly enhanced. The optimal GO-loaded amount was prove to be 10 mg, with the formation a highest NO removal rate of about 50 % for continous oxidizing NO. Nevertheless, further increasing the amount of GO resulted in the decrease of the activity. To the case of 30-GO/NH_2-MIL-125(Ti), it took about 1 h to obtain a stable NO removal rate (33 %), much lower than that of the optimal sample. We also traced the activity of the mechnical mixing sample (M10-GO/NH_2-MIL-125(Ti)) for better comparison. As shown in Fig. 8a, it was found that loading GO in the sample of M10-GO/NH_2-MIL-125(Ti) cannot effectively improve the activity of NH_2-MIL-125(Ti) via a mechanical mixing process. Comapred to the pure NH_2-MIL-125(Ti) sample, just slight increase of activity was observed. This suggested that the strong interaction between GO and NH_2-MIL-125(Ti), owing to the microwave solvothermal treatment, is the key to enhancing the activity for the strong capability to transfer the photo-generated electrons. Thus, it is reasonable that such excellent activity of the as-formed GO/NH_2-MIL-125(Ti) may be asscribed to the enhanced photo-generated electron transfer rate, low electron-hole recombination rate, and large surface area. For exploring the application in enviromental remediation, the as-prepared samples were also utilized to treat gaseous acetaldehyde pollutants. As shown in Fig.

8b, the sample of 10-GO/NH_2-MIL-125(Ti) shows a high activity for oxidizing gaseous acetaldehyde under visible light irradiation with about 65 % removal rate. Such value is much higher than that (48 %) of the pure NH_2-MIL-125(Ti). Similar to the results of the photocatalytic oxidation of NO, the mechanical mixing sample (M10-GO/NH_2-MIL-125(Ti)) still exhibited a lower photocatalytic performance for oxidizing acetaldehyde owing to the weak interaction between GO and NH_2-MIL-125(Ti), with the comparison to the sample prepared *via* microwave solvothermal process. For better understanding a possible working mechanism of GO/NH_2-MIL-125(Ti) for treating gaseous pollutants was prosed in Scheme 1. Upon being irradiated with visible light, the ligand linker, (H_2ATA), in the MOF crystals was excited for generating electrons, which can further transfer to the center of the Ti-O clusters for reducing Ti^{4+} to Ti^{3+}.[59] Owing to the strong heterojunctions between GO and NH_2-MIL-125(Ti), such trapped electrons in the clusters can be fast accumulated on the surface of GO nanosheets, allowing more electrons to react with the O_2 molecules for producing oxygen radicals ($\bullet O_2^-$). Thus, both the NO_x and organic pollutants could be further oxidized by these oxygen radicals for its strong oxidizing ability.

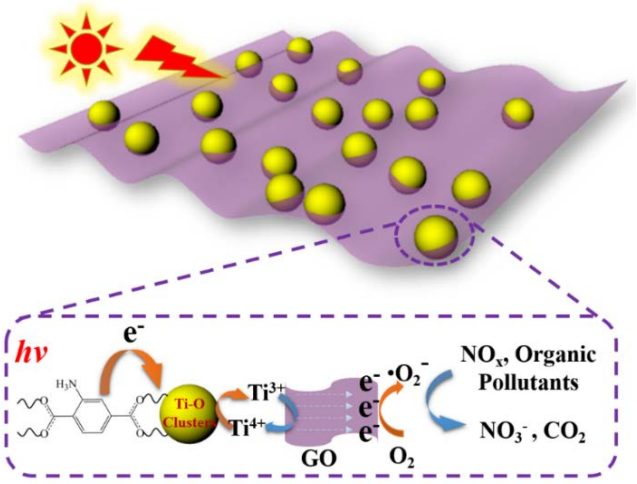

Scheme 3. The mechanism of GO/NH_2-MIL-125(Ti) for treating pollutants under visible light irradiation.

Chapter 4 Conclusion and Outlook

Highly crystallized NH_2-MIL-125(Ti) were *in-situ* dispersedly grafted on the suface of GO under the help of the hot-spot effcet of GO under the mcirowave irradiation. Strong intereraction between GO and NH_2-MIL-125(Ti) was obtained for the formation of heterojunctions. Both the high crystallinity and strong heterojunctions are highly

favarable for enhancing photocurrent, electron carrier density and electron-tranfer rate from NH_2-MIL-125(Ti) to GO, and for inhibiting the electron-hole recombination for achieving high quantum efficiency. Under visible-light ($\lambda > 420$ nm) irradiation, the electrons generated from NH_2-MIL-125(Ti) could be fast transfered to GO through the heterojunctions. The trapped electrons on GO could further react with O_2 for the formation of oxygen radicals, allowing the oxidation of NO_x and acetaldehyde. The present work also supplied a microwave-induced platform for the fabrication of carbon materials enhanced MOF photocatalysts with highly efficient optical and electronic property.

For the future work, we plan to optimize the synthesis route of this hybrid MOF material to achieve the best performance. Besides we will also applied the material into more applications, such as the removal of other gaseous pollutants and dye degradation. We also can take advantage of the microwave assisted synthesis to synthesize more novel MOF materials. Further we can calcinate the MOF materials under nitrogen to prepare TiC porous structure with large surface area.

Reference

1. A. Fujishima, *nature*, 1972, **238**, 37-38.
2. I. Paramasivam, H. Jha, N. Liu and P. Schmuki, *Small*, 2012, **8**, 3073-3103.
3. A. L. Linsebigler, G. Lu and J. T. Yates Jr, *Chemical reviews*, 1995, **95**, 735-

758.

4. C.-H. Wu and C.-L. Chang, *Journal of hazardous materials*, 2006, **128**, 265-272.

5. I. T. Peternel, N. Koprivanac, A. M. L. Božić and H. M. Kušić, *Journal of hazardous materials*, 2007, **148**, 477-484.

6. N. Daneshvar, D. Salari and A. Khataee, *Journal of Photochemistry and Photobiology A: Chemistry*, 2004, **162**, 317-322.

7. F. Zhang, X. Zhu, J. Ding, Z. Qi, M. Wang, S. Sun, J. Bao and C. Gao, *Catalysis letters*, 2014, **144**, 995-1000.

8. J. Lyu, L. Zhu and C. Burda, *ChemCatChem*, 2013, **5**, 3114-3123.

9. P. Akhter, M. Hussain, G. Saracco and N. Russo, *Fuel*, 2015, **149**, 55-65.

10. C. Adán, J. Marugán, S. Obregón and G. Colón, *Catalysis Today*, 2015, **240**, 93-99.

11. S. Caillol, *Journal of Photochemistry and Photobiology C: Photochemistry Reviews*, 2011, **12**, 1-19.

12. B. Hauchecorne and S. Lenaerts, *Journal of Photochemistry and Photobiology C: Photochemistry Reviews*, 2013, **14**, 72-85.

13. C. Baukal, *Metal finishing*, 2005, **103**, 18-24.

14. J.-R. Li, R. J. Kuppler and H.-C. Zhou, *Chemical Society Reviews*, 2009, **38**, 1477-1504.

15. H. Guo, F. Lin, J. Chen, F. Li and W. Weng, *Applied Organometallic Chemistry*, 2015, **29**, 12-19.

16. J. Lee, O. K. Farha, J. Roberts, K. A. Scheidt, S. T. Nguyen and J. T. Hupp, *Chemical Society Reviews*, 2009, **38**, 1450-1459.

17. L. J. Murray, M. Dinca and J. R. Long, *Chemical Society Reviews*, 2009, **38**, 1294-1314.

18. K. Sumida, D. L. Rogow, J. A. Mason, T. M. McDonald, E. D. Bloch, Z. R. Herm, T.-H. Bae and J. R. Long, *Chemical Reviews*, 2012, **112**, 724-781.

19. J.-R. Li, J. Sculley and H.-C. Zhou, *Chemical Reviews*, 2012, **112**, 869-932.

20. D.-X. Xue, Y. Belmabkhout, O. Shekhah, H. Jiang, K. Adil, A. J. Cairns and M. Eddaoudi, *Journal of the American Chemical Society*, 2015, **137**, 5034-5040.

21. Z.-G. Gu, W.-Q. Fu, X. Wu and J. Zhang, *Chemical Communications*, 2016, **52**, 772-775.

22. L. E. Kreno, K. Leong, O. K. Farha, M. Allendorf, R. P. Van Duyne and J. T. Hupp, *Chemical Reviews*, 2012, **112**, 1105-1125.

23. Y.-H. Han, C.-B. Tian, Q.-H. Li and S.-W. Du, *Journal of Materials Chemistry C*, 2014, **2**, 8065-8070.

24. C. Hou, J. Peng, Q. Xu, Z. Ji and X. Hu, *RSC Advances*, 2012, **2**, 12696-12698.

25. W.-w. Zhan, Q. Kuang, J.-z. Zhou, X.-j. Kong, Z.-x. Xie and L.-s. Zheng, *Journal of the American Chemical Society*, 2013, **135**, 1926-1933.

26. M. Dan-Hardi, C. Serre, T. Frot, L. Rozes, G. Maurin, C. Sanchez and G. Ferey, *Journal of the American Chemical Society*, 2009, **131**, 10857-+.

27. M. A. Nasalevich, R. Becker, E. V. Ramos-Fernandez, S. Castellanos, S. L. Veber, M. V. Fedin, F. Kapteijn, J. N. H. Reek, J. I. van der Vlugt and J. Gascon,

Energy & Environmental Science, 2015, **8**, 364-375.

28. N. D. McNamara, G. T. Neumann, E. T. Masko, J. A. Urban and J. C. Hicks, *Journal of Catalysis*, 2013, **305**, 217-226.

29. D. Jin, Q. Xu, L. Yu and X. Hu, *Microchimica Acta*, 2015, **182**, 1885-1892.

30. M. Tsuji, M. Hashimoto, Y. Nishizawa, M. Kubokawa and T. Tsuji, *Chemistry–A European Journal*, 2005, **11**, 440-452.

31. D. R. Baghurst and D. M. P. Mingos, *J. Chem. Soc., Chem. Commun.*, 1992, 674-677.

32. A. D. Salts, *The Photoredox Catalyzed Meerwein Arylation*, 23.

33. H. Kingston, *Atomic Spectrosc*, 1998, **2**, 27-30.

34. R. Gedye, F. Smith, K. Westaway, H. Ali, L. Baldisera, L. Laberge and J. Rousell, *Tetrahedron letters*, 1986, **27**, 279-282.

35. R. J. Giguere, T. L. Bray, S. M. Duncan and G. Majetich, *Tetrahedron letters*, 1986, **27**, 4945-4948.

36. M. B. Gawande, V. D. Bonifácio, R. Luque, P. S. Branco and R. S. Varma, *Chemical Society Reviews*, 2013, **42**, 5522-5551.

37. M. B. Gawande, V. D. Bonifácio, R. Luque, P. S. Branco and R. S. Varma, *ChemSusChem*, 2014, **7**, 24-44.

38. V. Polshettiwar and R. S. Varma, *Chemical Society Reviews*, 2008, **37**, 1546-1557.

39. M. B. Gawande and P. S. Branco, *Green Chemistry*, 2011, **13**, 3355-3359.

40. V. Polshettiwar and R. S. Varma, *The Journal of organic chemistry*, 2007, **72**,

7420-7422.

41. M. B. Gawande, P. S. Branco and R. S. Varma, *Chemical Society Reviews*, 2013, **42**, 3371-3393.

42. V. Polshettiwar and R. S. Varma, *Green Chemistry*, 2010, **12**, 743-754.

43. J. Liu, H. Bai, Y. Wang, Z. Liu, X. Zhang and D. D. Sun, *Advanced Functional Materials*, 2010, **20**, 4175-4181.

44. N. Zhang, Y. Zhang, X. Pan, M.-Q. Yang and Y.-J. Xu, *Journal of Physical Chemistry C*, 2012, **116**, 18023-18031.

45. C. Wang, X. Han, P. Xu, X. Zhang, Y. Du, S. Hu, J. Wang and X. Wang, *Applied Physics Letters*, 2011, **98**.

46. K. S. Kumar, S. Pittala, S. Sanyadanam and P. Paik, *Rsc Advances*, 2015, **5**, 14768-14779.

47. D. Q. Zhang, G. S. Li, X. F. Yang and J. C. Yu, *Chemical Communications*, 2009, DOI: 10.1039/b907963g, 4381-4383.

48. M. Wen, P. Liu, S. Xiao, K. Mori, Y. Kuwahara, H. Yamashita, H. Li and D. Zhang, *Rsc Advances*, 2015, **5**, 11029-11035.

49. D. C. Marcano, D. V. Kosynkin, J. M. Berlin, A. Sinitskii, Z. Sun, A. Slesarev, L. B. Alemany, W. Lu and J. M. Tour, *Acs Nano*, 2010, **4**, 4806-4814.

50. G. Li, B. Jiang, S. Xiao, Z. Lian, D. Zhang, J. C. Yu and H. Li, *Environmental Science-Processes & Impacts*, 2014, **16**, 1975-1980.

51. G. Li, D. Zhang, J. C. Yu and M. K. H. Leung, *Environmental Science & Technology*, 2010, **44**, 4276-4281.

52. Y. Fu, D. Sun, Y. Chen, R. Huang, Z. Ding, X. Fu and Z. Li, *Angewandte Chemie-International Edition*, 2012, **51**, 3364-3367.

53. G. Leofanti, M. Padovan, G. Tozzola and B. Venturelli, *Catalysis Today*, 1998, **41**, 207-219.

54. G. Li, D. Zhang and J. C. Yu, *Chemistry of Materials*, 2008, **20**, 3983-3992.

55. S. Park, K.-S. Lee, G. Bozoklu, W. Cai, S. T. Nguyen and R. S. Ruoff, *Acs Nano*, 2008, **2**, 572-578.

56. W. Zhu, P. Liu, S. Xiao, W. Wang, D. Zhang and H. Li, *Applied Catalysis B-Environmental*, 2015, **172**, 46-51.

57. M. Nara, H. Torii and M. Tasumi, *Journal of Physical Chemistry*, 1996, **100**, 19812-19817.

58. M. S. Dresselhaus, A. Jorio, M. Hofmann, G. Dresselhaus and R. Saito, *Nano Letters*, 2010, **10**, 751-758.

59. J. Xu, S. He, H. Zhang, J. Huang, H. Lin, X. Wang and J. Long, *Journal of Materials Chemistry A*, 2015, **3**, 24261-24271.

60. D. Sun, L. Ye and Z. Li, *Applied Catalysis B-Environmental*, 2015, **164**, 428-432.

61. J. Yu, J. Jin, B. Cheng and M. Jaroniec, *Journal of Materials Chemistry A*, 2014, **2**, 3407-3416.

62. L. Jia, D.-H. Wang, Y.-X. Huang, A.-W. Xu and H.-Q. Yu, *Journal of Physical Chemistry C*, 2011, **115**, 11466-11473.

63. Y. Zhu, S. Murali, W. Cai, X. Li, J. W. Suk, J. R. Potts and R. S. Ruoff, *Advanced*

Materials, 2010, **22**, 3906-3924.

64. G. Li, L. Wu, F. Li, P. Xu, D. Zhang and H. Li, *Nanoscale*, 2013, **5**, 2118-2125.

65. H. X. Li, G. S. Li, J. Zhu and Y. Wan, *Journal of Molecular Catalysis a-Chemical*, 2005, **226**, 93-100.

66. L. Q. Jing, Y. C. Qu, B. Q. Wang, S. D. Li, B. J. Jiang, L. B. Yang, W. Fu, H. G. Fu and J. Z. Sun, *Solar Energy Materials and Solar Cells*, 2006, **90**, 1773-1787.